



NJC

Naphthalene Flanked Diketopyrrolopyrrole Based Organic Semiconductors for High Performance Organic Field Effect Transistors

Journal:	<i>New Journal of Chemistry</i>
Manuscript ID	NJ-ART-03-2018-001453.R1
Article Type:	Paper
Date Submitted by the Author:	02-Jun-2018
Complete List of Authors:	<p>Sonar, Prashant; Queensland University of Technology , School of Chemistry, Physics and Mechanical Engineering Sun, Huabin ; Dongguk University Liu, Qian; Queensland University of Technology Faculty of Science and Engineering, Chemistry, Physics and Mechanical Engineering Noh, Yong-Young; Dongguk University, Blaikie, Chula; Queensland University of Technology Faculty of Science and Engineering Caporale, Chiara; Curtin University - Perth City Campus Manzhos, Sergei; National University of Singapore, Mechanical Engineering Feron, Krishna; University of Newcastle, Centre for Organic Electronics MacLeod, Jennifer; INRS, Univ. of Quebec, Energy, Materials and Telecommunications Massi, Massimiliano; Curtin University , Chemistry Bottle, Steven; Queensland University of Technology Brisbane, School of Physical and Chemical Sciences Bell, John; Queensland University of Technology, Faculty of Built and Engineering</p>

Naphthalene Flanked Diketopyrrolopyrrole Based Organic Semiconductors for High Performance Organic Field Effect Transistors

Qian Liu,^a Huabin Sun,^b Chula Blaikie,^a Chiara Caporale,^c Sergei Manzhos,^d Krishna Feron,^{e,f}
Jennifer M. MacLeod,^a Massimiliano Massi,^c Steven E. Bottle,^a John Bell,^a Yong-Young
Noh*^b and Prashant Sonar*^a

^a School of Chemistry, Physics and Mechanical Engineering (CPME), Queensland University of Technology (QUT), Brisbane, QLD 4000, Australia.

^b Department of Energy & Materials Engineering, Dongguk University, Seoul 04620, Republic of Korea.

^c Department of Chemistry, Curtin University, GPO Box U1987, Perth 6845, Western Australia.

^d Department of Mechanical Engineering, Faculty of Engineering, National University of Singapore Block EA #07-08, 9 Engineering Drive 1 117576, Singapore.

^e CSIRO Energy Centre, 10 Murray Dwyer Circuit, Mayfield West, NSW 2304, Australia.

^f Centre for Organic Electronics, University of Newcastle, Callaghan, NSW 2308, Australia.

Yong-Young Noh: yynoh@hotmail.com

Prashant Sonar: sonar.prashant@qut.edu.au

Here, we design and synthesize three new diketopyrrolopyrrole (DPP) derivatives with naphthalene, possessing large-scaled π -delocalized electronic structure, as the flanking groups and both linear (*n*-decyl and *n*-dodecyl) and branched (2-hexyldecyl) alkyl chains as substitutions as active layer for high performance organic field-effect transistors (OFETs). The thermal, photophysical properties, energy levels and solid state molecular stacking have

been studied in detail. All the materials show excellent thermal stability with a decomposition temperature of up to near 400 °C, high semi-crystallinity feature, suitable HOMO & LUMO energy levels, and varying crystalline domain sizes in thin films. Bottom-contact/top-gate transistor devices are thus fabricated to investigate the mobility. Encouragingly, all compounds function well in OFET devices and show significant potential as *p*-type semiconducting materials. The monomer with the *n*-decyl alkyl chain (D-DPPN) shows the highest mobility of 0.019 cm² V⁻¹ s⁻¹, with the $I_{\text{on}}/I_{\text{off}}$ ratio reaching 10⁶. We first synthesize naphthalene flanked DPP monomers and achieve high mobility in OFET devices when using these monomers without any further functionalization as semiconductors directly. The primary result that high mobility is observed for monomers only opens a new way for further DPP application and provides more possibilities to constructing high performance polymeric and small molecular semiconductors based on this new DPP dye.

Introduction

Solution-processable organic field-effect transistors (OFET) have been attracting considerable research attention on account of their potential applications as cost-effective components in large-area flexible displays, smart cards, logic circuits, sensors and radio frequency identification (RFID) tags.¹⁻⁶ As a solution-processing technique, organic semiconducting materials play a significant role in promoting the advances of OFET.^{7,8} Consequently, great efforts in materials design have boosted the OFET mobility values achievable from both semiconducting polymers and small molecules up to near 1 cm² V⁻¹ s⁻¹.⁷⁻¹⁵ Furthermore, several recent papers have reported that mobility values surpassing 10 cm² V⁻¹ s⁻¹ can be obtained.^{16,17} In spite of the numerous milestone achievements for OFET devices in the last 10 years, it remains a challenge to develop new molecular systems suitable for transistor applications because many synthesized materials did not work or showed very

low mobility in OFET devices, and most high mobility OFET materials were achieved through slight modification of the existing semiconductors with high performance mainly by changing one of the alternative building blocks in polymeric materials or replacing the flexible side chains of workable polymers or small molecules.¹⁸⁻²⁰

In the field of designing high performance OFET materials, two approaches have been mostly used. As the carrier transport in organic molecular films is intrinsically governed by the extent of intermolecular orbital coupling which determines the charge transfer integral,^{11,21} the first promising approach is to develop highly π -extended molecules.^{12,22-24} As an example, materials based on picene, di(thienothienyl)ethylene (DTTE), or dinaphtho[2,3-*b*:2',3'-*f*]thieno[3,2-*b*]thiophene (DNFT) that all have highly π -conjugated structures have shown high performance in OFET devices with mobility exceeding $1 \text{ cm}^2 \text{ V}^{-1} \text{ s}^{-1}$.²⁵⁻²⁹ Another effective approach is to utilize the self-assembly nature of organic molecules in solid state that in which molecular ordering is strongly influenced by flexible alkyl groups. Thus the self-assembly of materials has been widely studied through side chain engineering from different molecular systems like diketopyrrolopyrrole (DPP), isoindigo and truxene and this has proved to be a powerful design strategy.³⁰⁻³⁸ In the present work, these two factors are considered with the aim of designing new organic semiconducting materials for OFET devices.

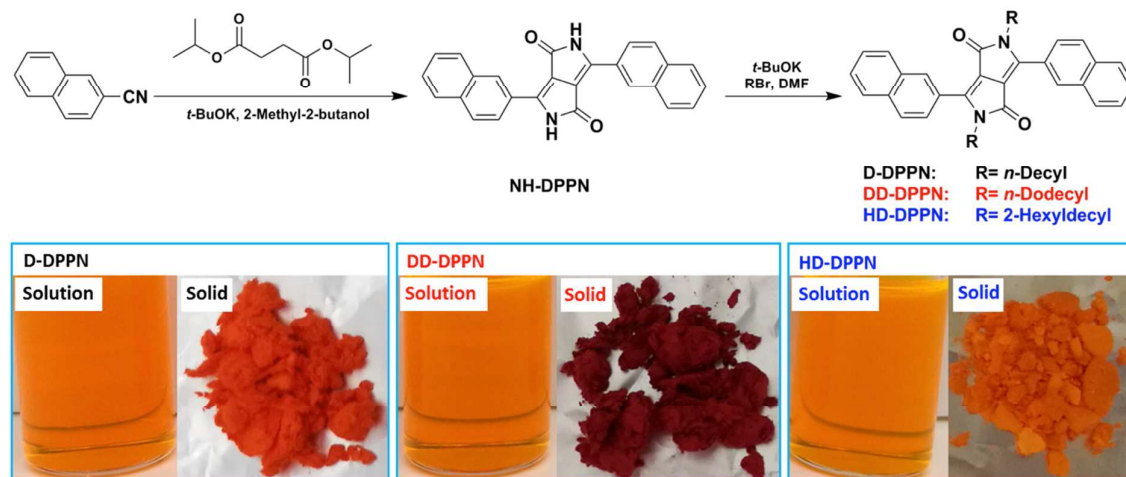
DPP is a well-known, much-utilized and recently widely-studied promising building block for designing new high performance donor-acceptor-based conjugated functional materials for both organic photovoltaic (OPV) and OFET devices.³⁹⁻⁴⁸ DPP is a fused aromatic semiconducting moiety with several favourable features.⁴⁶ Importantly for use in OFET materials, the DPP motif is able to not only contribute to tight π - π stacking but also enhance the charge delocalization of corresponding compounds owing to its high level of co-planarity and quinoidal structure, which is highly beneficial to charge-carrier transport through

intermolecular charge hopping.⁴⁹ As a result, DPP-based materials have demonstrated some of the highest hole mobility values for OFET devices to date.^{16,17} Given the requirements of high degree of conjugation and rigidity, favouring enhanced π - π overlap in solid state, fused compounds are preferred flanking groups when designing materials for OFET applications.¹² Naphthalene, which has an acene structure, has been a widely introduced moiety to design π -extended structural polymers and small molecules in organic electronics, and impressive device performance was observed when using these materials as an active semiconductors in OPV and OFET devices.^{24,50-57} According to the strategies discussed above for designing high performance OFET semiconductors, combining DPP with naphthalene to achieve a new class of DPP family could be a novel approach and such attempt has not been reported so far. This approach may produce highly promising conjugated functional materials for OFET devices. To guarantee solution processibility, different flexible alkyl chains can be attached to the nitrogen atom of the DPP core for making printable semiconductors for large area devices. Earlier studies have shown that side-chain engineering can significantly affect molecular packing and the π -coplanarity of DPP based materials, in addition to its conventional role as a solubilizer,^{33,36,37} therefore side chain selection is as important as manipulating the conjugated backbones. Both linear and branched alkyl chains were selected to make an integrated comparison in this work.

Based on the above ideas, we designed and synthesized a new DPP derivative with naphthalene as the flanking group (DPPN) with either linear (*n*-decyl or *n*-dodecyl) or branched (2-hexyldecyl) alkyl chains as the side substitutions, being named D-DPPN, DD-DPPN, and HD-DPPN (structures are given in **Scheme 1**), respectively. The thermal, optical, solid state stacking and electronic properties of these three simple core compounds or monomers have been studied in detail. Bottom-contact/top-gate OFET devices were fabricated using all three materials as active channel semiconductors in order to study their

structure-property relationship. The OFET devices exhibit promising performance with a highest hole mobility of $0.019 \text{ cm}^2 \text{ V}^{-1} \text{ s}^{-1}$ for monomeric unit with straight short decyl alkyl chain substituted D-DPPN. Notably, the molecule used directly in the device is only alkylated naphthalene DPP monomer without any further functionalization. Other materials of the series with straight and branched alkyl chain substituted DPPN, namely, DD-DPPN and HD-DPPN also show moderate hole mobility values of 0.0012 and $0.0008 \text{ cm}^2 \text{ V}^{-1} \text{ s}^{-1}$, respectively. These results demonstrate that naphthalene flanked DPP (DPPN) is a promising candidate for high performance OFET materials. Currently, our group is working on DPPN-containing small molecules and polymers for various organic electronic devices. This work clearly provides new molecular design guidelines for synthesizing new DPP based fused aromatic conjugated building blocks for future high performance printable devices.

Results and Discussion



Scheme 1 Synthetic routes to D-DPPN, DD-DPPN, HD-DPPN and their solution and solid appearance.

Synthesis and Characterization:

The synthesis of the three small molecules is depicted in **Scheme 1**. Starting from cyano naphthalene, the most important intermediate (NH-DPPN) was prepared in one step at a yield of more than 60%. This reaction was performed referring to the previously reported procedure used for the synthesis of thiophene flanked DPP monomer.⁴⁶ The final compounds, D-DPPN, DD-DPPN and HD-DPPN, were synthesized by the alkylation reaction of NH-DPPN with three different brominated alkyl chains using potassium tert-butoxide (*t*-BuOK) as a base in *N,N*-Dimethylformamide (DMF) as solvent. The resulting materials are characterized by ¹H NMR, ¹³C NMR spectroscopy and high resolution mass spectrometry (HRMS). Both the NMR and HRMS spectra are shown in supporting information. The three synthesized DPPN molecules are soluble in commonly used organic solvents such as tetrahydrofuran (THF), dichloromethane (DCM), chloroform (CF), and chlorobenzene (CB) which is required for fabricating solution-processible OFET devices.

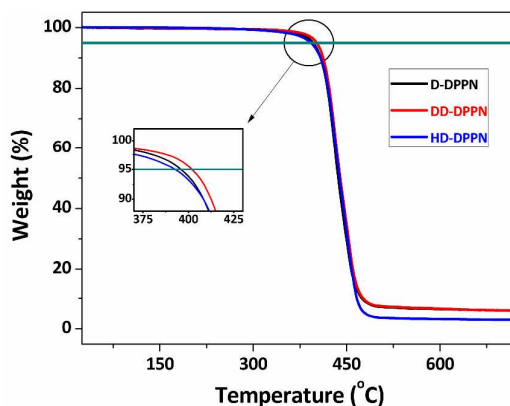


Fig. 1 TGA thermograms of D-DPPN, DD-DPPN and HD-DPPN.

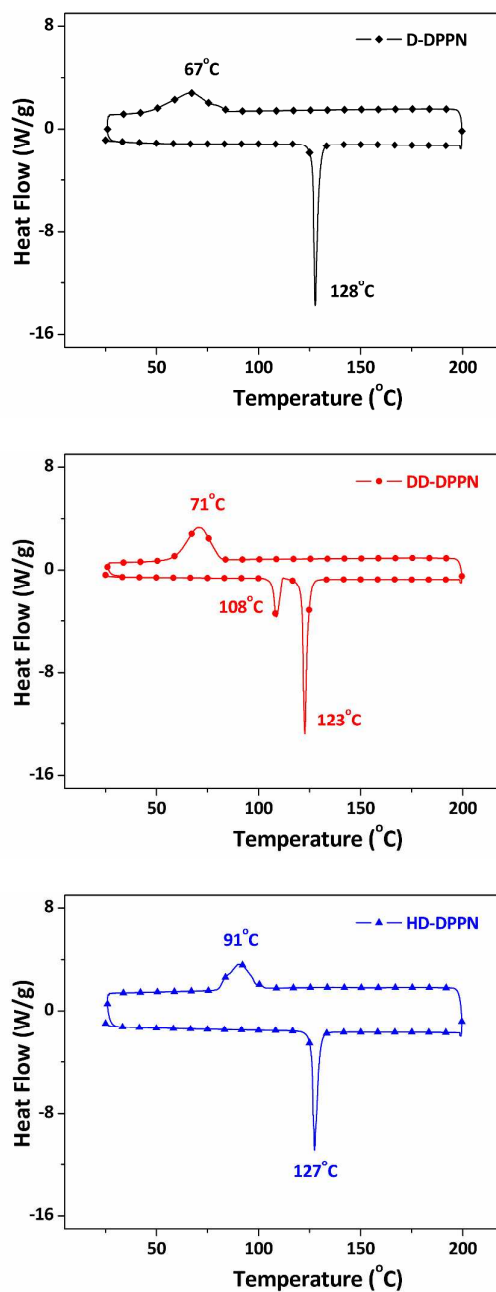


Fig. 2 DSC analysis of D-DPPN, DD-DPPN and HD-DPPN.

Thermal Properties:

The thermal behaviour of D-DPPN, DD-DPPN and HD-DPPN compounds were investigated by thermogravimetric analysis (TGA) and differential scanning calorimetry (DSC). As shown in **Fig. 1**, the TGA study indicates that all three DPP derivatives possess excellent thermal

stability in nitrogen atmosphere with a decomposition temperature (T_d , 5% weight loss) of 396 °C for D-DPPN, 402 °C for DD-DPPN and 393 °C for HD-DPPN, which is high enough for applications of these materials in OFET (current case) or other organic electronic devices. The DSC analysis (**Fig. 2**) shows that all the DPPN based compounds exhibit crystalline isotropic melting transitions. During heating scans, all three compounds display similar melting points at 128 °C for D-DPPN, 123 °C for DD-DPPN and 127 °C for HD-DPPN, respectively. Combined with the similar T_d , it demonstrates that the alkyl chains (either straight or branched one) has little impact on thermal properties. During the cooling process, characteristic phase transition behaviour appears at 67 °C, 71 °C and 91 °C for D-DPPN, DD-DPPN, and HD-DPPN, respectively. The HD-DPPN with branched side chain shows higher crystallinity than the linear ones that is attributed to the less steric hindrance caused by the smaller dihedral angles between naphthalene and DPP units (see the DFT results). Interestingly, DD-DPPN, functionalized with linear dodecane, exhibits a dual melting transition suggesting there are some isolated microcrystals that can be observed in the polarized microscope images (**Fig. 10**) while D-DPPN and HD-DPPN show continuous crystalline domains.⁵⁸ The characterized crystallinity of these three monomers strongly suggests the possibility to use them directly in OFET devices while the good thermal stability can effectively prevent the degradation of active layer.

Table 1 Summary of photophysical data.

Complex	Analysis	Absorption			Emission ^c	
		λ_{\max} (nm)	λ_{onset} (nm) E_g (eV)	λ_{em} (nm)	τ_{aer} ^d (ns)	Φ ^e
D-DPPN	Degas ^a	486, 324	---	558, 596	6.5	0.216
	Solid ^b	513, 329	610, 2.03	615	1.1 (70) 4.7 (30)	---
DD-DPPN	Degas ^a	486, 324	---	558, 596	6.7	0.209
	Solid ^b	527, 324	612, 2.03	565, 615	2.3 (26) 5.4 (74)	---
HD-DPPN	Degas ^a	482, 323	---	558, 596	6.6	0.206
	Solid ^b	510, 332	546, 2.27	540, 574	0.6 (82) 3.3 (18)	---

^a Measured from degassed solution (ca. 10^{-5} M). ^b Film obtained by evaporation of the complex solution. ^c $\lambda_{\text{exc}} = 330$ nm. ^d For the biexponential excited state lifetime (τ), the relative weights of the exponential curves are reported in parentheses. ^e Measured versus $\text{Ru}(\text{bpy})_3^{2+}$ in water ($\Phi_r = 0.028$).

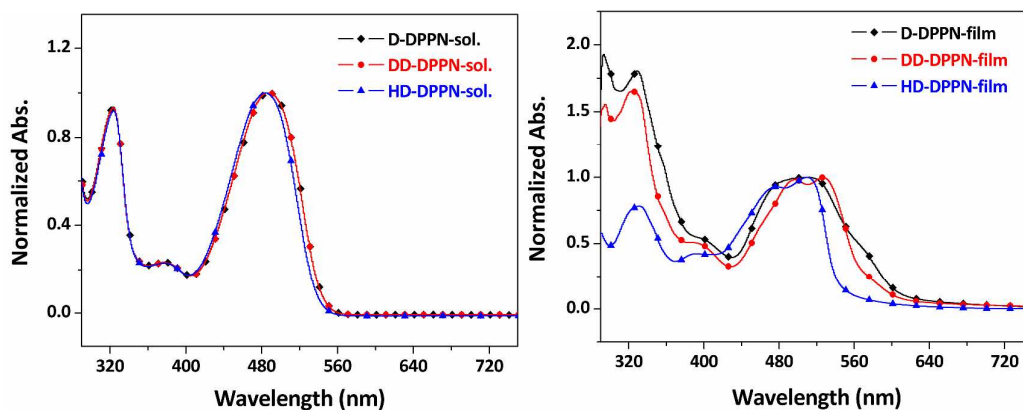


Fig. 3 UV-Vis absorption spectra of D-DPPN, DD-DPPN and HD-DPPN in both solutions and as thin films.

Photophysical Properties:

A summary of the photophysical data for the synthesized compounds is reported in **Table 1**. The normalized UV-Vis absorption spectra of N-alkyl substituted naphthalene DPP molecules obtained from both solutions and spin coated thin films are shown in **Fig. 3** and summarized in **Table 1**. As expected, the three spectra are virtually identical and exhibit two

absorption bands independently of the nature of the alkyl chain substituents. According to previous studies, the high energy band in the 270-360 nm region is attributed to π - π^* electronic transitions and the lower energy band in the 400-560 nm region originates from intramolecular charge transfer (ICT) transitions. In solution, the vibronic structure is not well-defined in the ICT absorption band that is ascribed to the large torsion between naphthalene and DPP which causes poor co-planarity and thus lower conjugation. For the thiophene and furan analogues that both have less than 2° dihedral angle, the 0-0 and 0-1 vibronic transitions are much more pronounced while for benzene counterpart that has similar dihedral angle ($\sim 40^\circ$) with our naphthalene DPP, the vibronic structure is not well-defined neither.⁵⁹ Going from solution to thin films, it is noted that all compounds show a red shift for the ICT peak that is due to the formation of J-aggregation.^{47,60} What's more, shoulder peaks are observed in 470 - 500 nm for all three materials that is from the H-aggregation formed by sliding the intermolecular π - π stacking.⁴⁷ From the spectra, we can clearly see that D-DPPN shows almost equal intensity for J and H aggregation while DD-DPPN and HD-DPPN show stronger J aggregation that is disfavoured for the carrier transport because J-type molecular packing are more slipped than H-type aggregation in the π - π stacking direction.⁴⁷ The optical band gaps calculated from onset of films absorption are 2.03, 2.03 and 2.27 eV for D-DPPN, DD-DPPN and HD-DPPN, respectively (**Table 1**). Although the large dihedral angles cause less conjugation, the fused naphthalene groups extend the conjugated length that broaden the absorption and thus naphthalene DPP shows relatively smaller band gaps than its thiophene (2.18 eV) furan (2.23 eV) and benzene (2.39 eV) DPP analogues with butyl alkyl side chain.⁵⁹

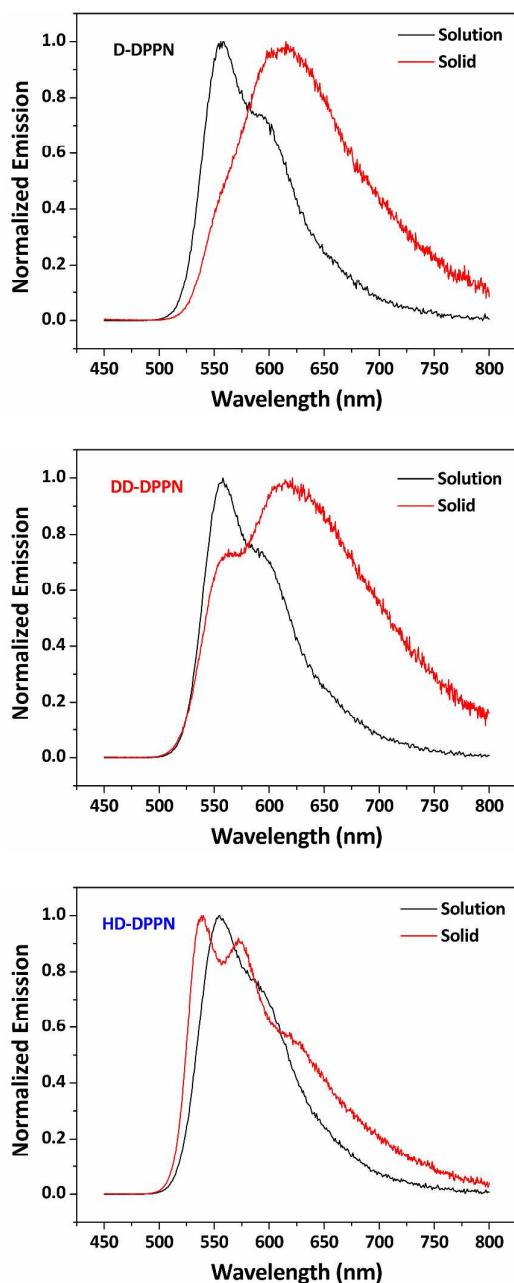
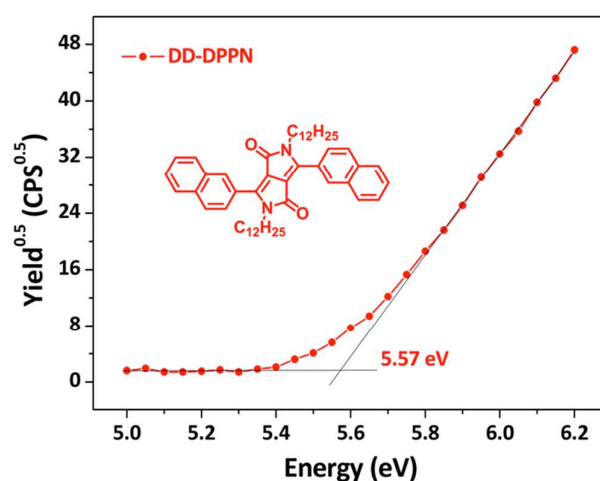
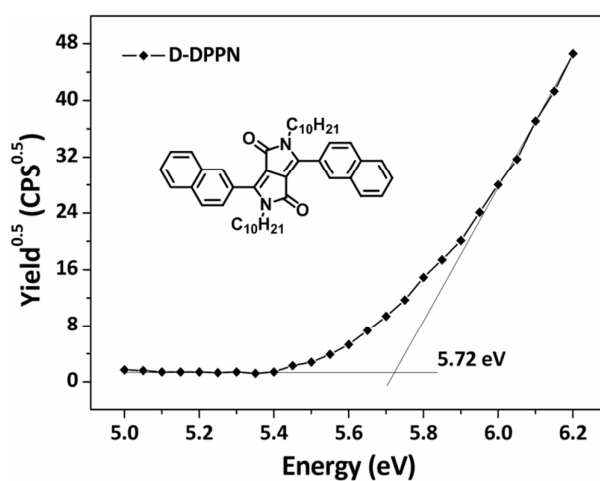


Fig. 4 Emission spectra of D-DPPN, DD-DPPN and HD-DPPN.

The emission profiles of these three compounds, measured from degassed dichloromethane solutions and thin films with excitation at 330 nm, are reported in **Fig. 4**. In solution, the slightly structured emission profiles do not appear to be dependent from the excitation wavelength, therefore the emission is ascribed to spin-allowed radiative decay from the

singlet ^1ICT excited state. This is also supported by the relatively fast and oxygen independent excited state lifetime decay with value around 6.5 ns (**Table 1**), which is similar for all the three compounds and satisfactorily fit by a monoexponential function from measurements in solution. The three compounds also have very similar values photoluminescence quantum yield, around 21% (**Table 1**), again indicating that the nature of the alkyl substituents has less effect on the photophysical properties in solution. The emission profiles from thin films appear visibly red-shifted in the case of D-DPPN and DD-DPPN due to aggregation. As previously noted in the absorption spectra, because of the blue-shift spectrum of HD-DPPN compared with D-DPPN and DD-DPPN and disfavoured aggregation, a less degree of red-shift is also observed in its emission spectrum.



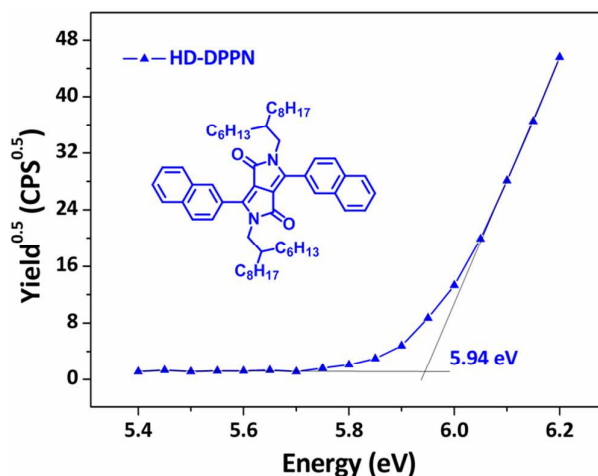


Fig. 5 Photoelectron spectroscopy in air (PESA) measurements of D-DPPN, DD-DPPN and HD-DPPN.

PESA and DFT Calculations:

The electronic structure of molecules not only plays an important role for charge injection and transport in organic semiconductors, but also is crucial for environmental stability. In terms of OFET devices, the voltage applied to the gate will shift up or down the energy levels of semiconductors with respect to the Fermi level (E_F) of the metal (gold or aluminium contacts) and thereby modulate the conductivity of the channel.¹¹ As a consequence, the energy levels including the highest occupied molecular orbital (HOMO) and lowest unoccupied molecular orbital (LUMO) are one of the most important properties of semiconductors which can not only instruct the selection of metal electrodes but can also broadly predict whether the materials are suitable for OFET devices. The HOMO values of the newly synthesized naphthalene DPP monomers were measured through photoelectron yield spectroscopy in air (PESA) and were determined to be -5.72, -5.57 and -5.94 eV for D-DPPN, DD-DPPN, and HD-DPPN, respectively (**Fig. 5**). The corresponding LUMO energy levels are estimated to be -3.69, -3.54 and -3.67 eV by assuming that the optical bandgap = LUMO - HOMO.

Obviously the linear side chain monomers have higher HOMO energy levels than the branched one, indicating the D-DPPN and DD-DPPN are more easy to form hole carrier charge transport path and thus higher hole mobility in OFET device. Generally the alkyl chains will have little effect on the electronic energy levels, which has been reported in literature for both polymers and small molecules.^{36,37,60} In current work, the small effect of chains on molecular properties is confirmed by the solution absorption peaks and DFT results (vide infra). The difference of HOMO and LUMO energy levels is due to the synergistic effect of the different torsional extent of the conjugated backbone and intermolecular stacking manner caused by the alkyl side chains.⁶¹

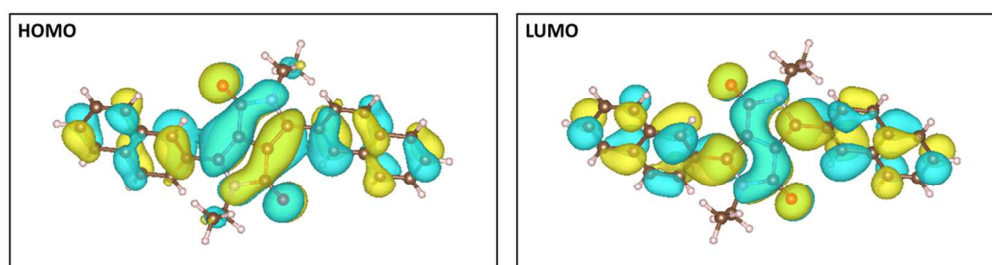


Fig. 6 the HOMO-LUMO distributions with ethyl side chains (they are similar for all chains studied here).

To clearly understand the torsional extent of conjugated backbone and get deeper insight to the intermolecular stacking of all the monomers, density functional theory (DFT) and powder X-ray diffraction (XRD) were carried out. DFT can not only investigate the energy level values but also molecular orbital distributions and dihedral angles between the DPP core and naphthalene flanking group. The DFT results show that the side chains have little influence on the distribution and energies of molecular orbitals (HOMO: -5.55, -5.53, -5.49 eV; LUMO: -2.80, -2.82, -2.85 eV). All the three monomers have similar highest occupied molecular orbital (HOMO) and lowest unoccupied molecular orbital (LUMO) shapes as shown in **Fig. 6** where the side chain was replaced with ethyl group (the orbitals are visually similar with

other chains). The dihedral angles between naphthalene and DPP core are determined to be 41° for D-DPPN, 38° for DD-DPPN and 33° for HD-DPPN. The side view of the molecules is shown in supporting information (Figure S10) where the dihedral angles can be observed clearly. This result further indicates that the different properties in thin film absorption, solid state emission and HOMO & LUMO energy levels are resulted from the different manners of molecular aggregation in solid state which can be visually observed from the solution and solid appearance in Scheme 1.

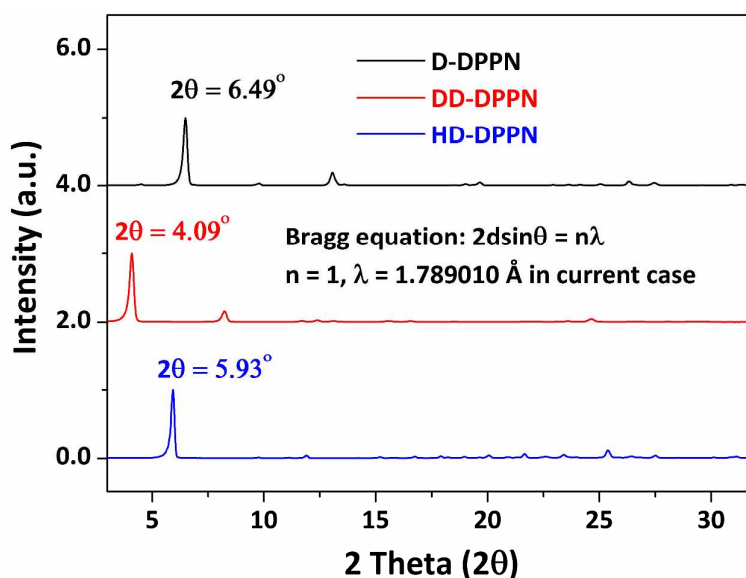
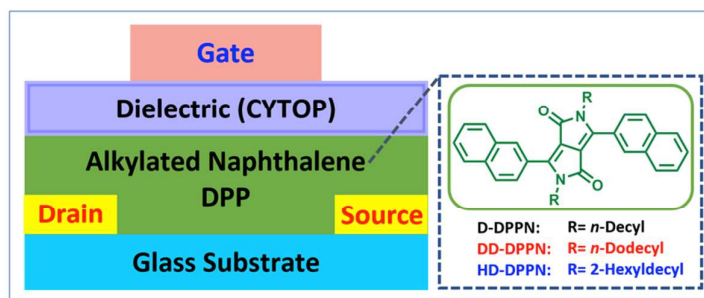


Fig. 7 XRD patterns of D-DPPN, DD-DPPN and HD-DPPN.

The powder XRD was used to measure the stacking behaviour of monomers in the solid state. As shown in Fig. 7, all compounds show sharp and clear diffraction peaks at $2\theta = 6.49^\circ$, 4.09° , and 5.93° for D-DPPN, DD-DPPN, and HD-DPPN, respectively, corresponding to an intermolecular lamellar distance of 15.80 \AA , 25.07 \AA , 17.29 \AA , respectively. It can be seen that the length of linear side chain has large influence on the intermolecular alkyl chain stacking. While for the branched one, although the hexyldecyl side chain is much more bulky than decyl and dodecyl chain, HD-DPPN shows similar lamellar distance with D-DPPN and

much shorter value than that of DD-DPPN indicating branched side chains are easy to form chain-chain interdigitation. D-DPPN and HD-DPPN also show a long-range stacking along the molecular backbones with several apparent peaks between $10-30^\circ$, which is helpful to form a continuous phase structure in solid state. Comparatively, DD-DPPN shows a much cleaner XRD pattern. The XRD results are consistent with the notion that the alkyl side chains can greatly influence the packing orientation of molecules in solid state, which can impact the π -electron delocalization and thus cause changes of energy levels.

Fabrication of Solution-processed OFET Devices:



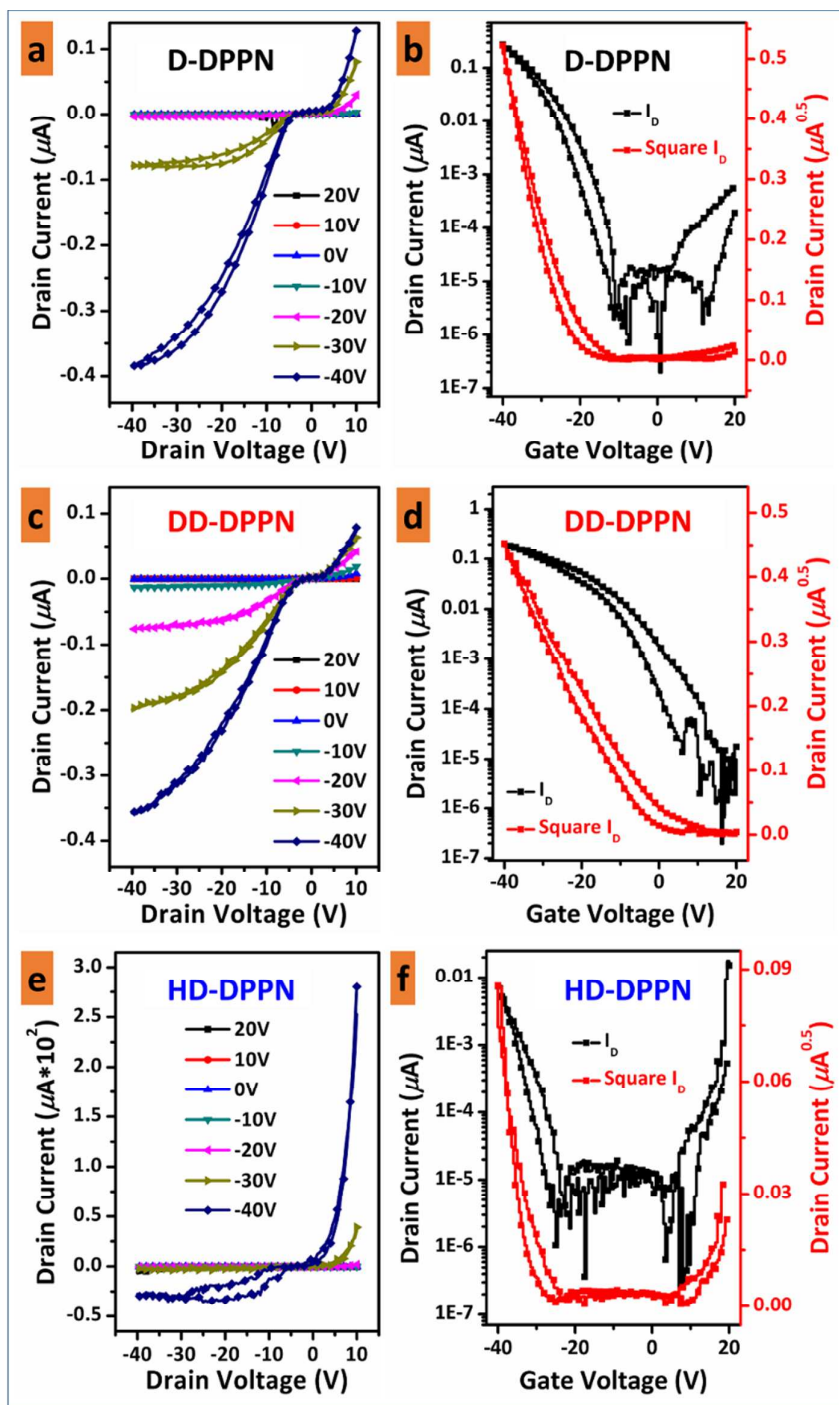


Fig. 8 Top gate bottom contact OFET device schematic and typical output (a, c, e) and transfer (b, d, f, $V_D = -40$ V) curves of D-DPPN (a, b), DD-DPPN (c, d) and HD-DPPN (e, f) based OFET devices after annealing at 100 °C.

The potential use of naphthalene-flanked DPP materials in organic electronics was investigated by measuring the mobilities of OFETs fabricated by spin-coating with a top gate bottom contact structure device configuration on glass substrates where D-DPPN, DD-DPPN and HD-DPPN were used as active layers. **Fig. 8** shows the device schematic used in this study and the representative output and transfer curves after annealing at 100 °C. The OFET parameters of the devices annealed at 100 °C extracted from transfer curves of the saturation regime, including mobility values (μ^h), threshold voltage (V_{th}), and On/Off ratio (I_{On}/I_{Off}) are summarized in **Table 2**.

Table 2. Summary of OFET Performance.

Materials	Ann. Temp. (°C)	$\mu^h_{ave.} \times 10^{-2}$ (cm ² V ⁻¹ s ⁻¹)	$\mu^h_{max.} \times 10^{-2}$ (cm ² V ⁻¹ s ⁻¹)	V_{th} (V)	I_{On}/I_{Off} ($\times 10^6$)	GIXRD (2 θ)
D-DPPN	100	0.96±0.01	1.90	-20.1±1.9	1.05±1.00	3.93/5.64
DD-DPPN	100	0.08±0.04	0.12	-2.03±2.2	0.18±0.04	3.55/3.52
HD-DPPN	100	0.06±0.03	0.08	-27.8±0.2	0.04±0.01	---/5.14

The obtained data clearly demonstrate that the materials behave *p*-type transport as the hole accumulation for negative gate voltages. The hole mobility is calculated with data obtained in saturation regime. From the obtained OFET characteristics, it is clear that the nature of the flexible alkyl chain attached to nitrogen atoms has a strong impact on charge carrier transport. A shorter straight decyl-substituted DPPN compound (D-DPPN) based OFET device shows the best performance with the highest hole mobility of 0.019 cm² V⁻¹ s⁻¹. When the shorter straight alkyl chain was replaced by a longer one, dodecyl substituted DPPN compound (DD-DPPN) exhibits a lower hole mobility of 0.0012 cm² V⁻¹ s⁻¹. Furthermore, a longer branched hexyldecyl substituted DPPN compound (HD-DPPN) shows the lowest performance among all these materials with a hole mobility of 0.0008 cm² V⁻¹ s⁻¹. The differences in hole mobility values may result from both the varied molecular stacking as discussed below based on thin film grazing incidence X-ray diffraction (GIXRD) and based on thin film nanotopography as

discussed below using atomic force microscopy (AFM) and polarized microscope image. To find the charge transport behaviour difference between naphthalene and thiophene flanked DPP, we fabricated transistor based on thiophene DPP monomer with a branched butyloctyl alkyl chain, unfortunately, the device didn't work using the same conditions so we didn't explore further and didn't synthesize other alkylated thiophene flanked DPP monomers. According to our current results, the shorter the side chain, the higher the hole mobility. As per literature, thiophene and phenyl flanked DPP monomers with ethylhexyl and hexyl shorter side chains exhibits hole mobility values of 4×10^{-3} and $2 \times 10^{-4} \text{ cm}^2 \text{ V}^{-1} \text{ s}^{-1}$ respectively.^{62,63} Upon comparing the obtained charge carrier mobility results for our newly reported naphthalene flanked DPP in this work with that of previously reported thiophene and phenyl flanked DPP monomers, our naphthalene DPP exhibits charge carrier mobility in 10^{-2} range which is one and two orders of magnitude higher than thiophene and phenyl flanked DPP. This study clearly indicates that naphthalene flanked DPP is a highly promising candidature to create range of new *p*-type and relevant organic semiconductors.

None of the devices based on DPPN derivatives worked after 150 °C annealing, which may be due to the formation of isolated organic crystal films upon heating above to the melting temperature of the materials, as observed from polarized microscope images (see the following discussion in “microstructural analysis of monomer films” section). Upon heating to 150 °C, the thin films of DPPN derivatives D-DPPN, DD-DPPN and HD-DPPN melted first and then solidified during the cooling process which resulted in a poor thin-film nanostructure (see Figure S11 in supporting information). One of the major reasons for this phenomenon is attributed to the melting point and all materials melt below 150 °C. In additional experiments, devices fabricated on SiO₂/Si substrate failed to exhibit transistor behaviour.

Grazing Incidence X-ray Diffraction (GIXRD)

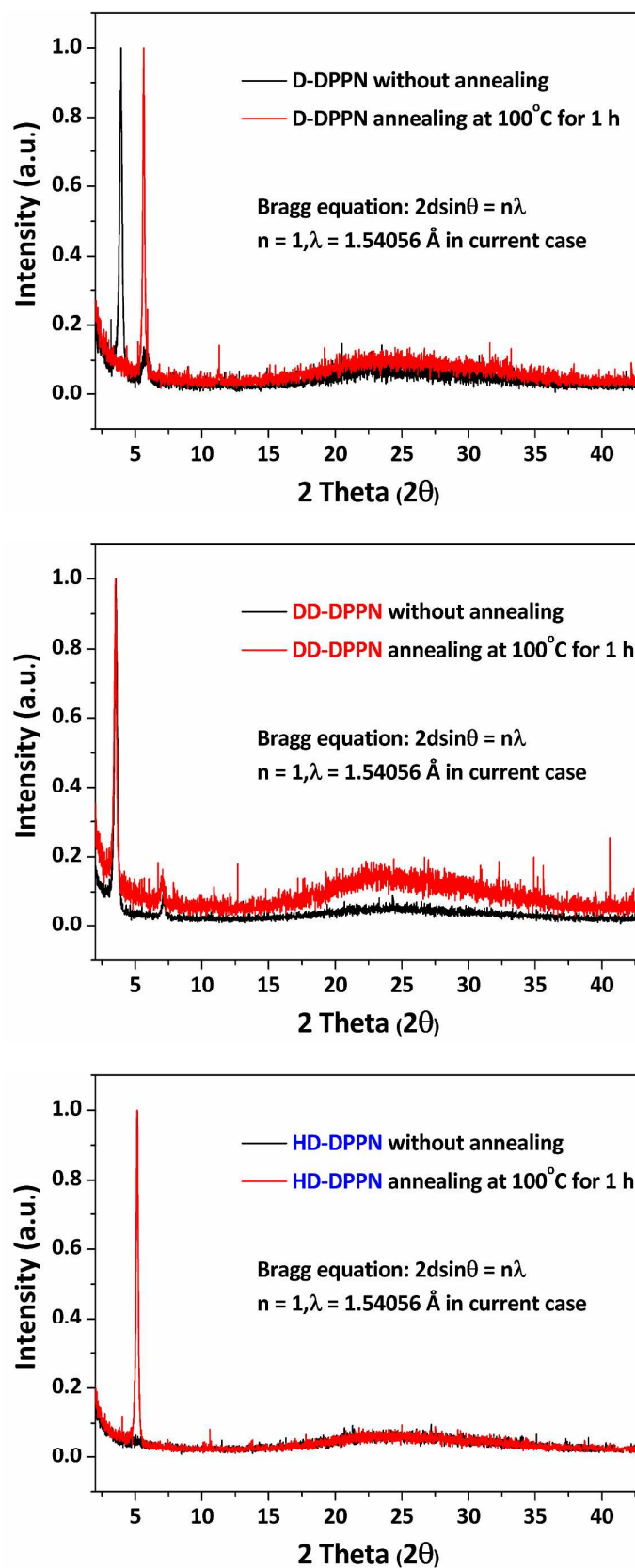


Fig. 9 thin films grazing incidence XRD patterns for D-DPPN, DD-DPPN and HD-DPPN.

Since the transistor devices are based on the thin films of D-DPPN, DD-DPPN and HD-DPPN active channel semiconductors, we performed the grazing incidence X-ray diffraction (GIXRD) study using these material's thin films without and with annealing at 100 °C for 1 h (similar to the device fabrication condition). From **Fig. 9** and **Table 2**, we can clearly see that the GIXRD results have the similar trend as like powder XRD. However, unlike polymers, it is hard to pull out a π - π stacking distance for small molecules. For our monomer, we can see weak peaks at around 25° in the GIXRD data and this is attributed to the reflection of π - π stacking. However, it is very hard to extract an exact value for these weak peaks. For D-DPPN and HD-DPPN, the short lamellar distances after 100 °C annealing (15.66 and 17.18 Å) indicate that there is a high degree of interchain interdigitation with each other around adjacent layers.⁹ Although the alkyl stacking directions are not directly linked to charge transport pathways, they are reflective of the overall degree of crystallinity and crystalline order. From the following polarized microscope images, we can see that D-DPPN and HD-DPPN can form continuous crystalline domains where D-DPPN with shorter lamellar distance shows larger domain size, while for DD-DPPN, some isolated organic crystals were observed that may be caused by the longer interchain distance.

Microstructural Analysis of Monomer Films:

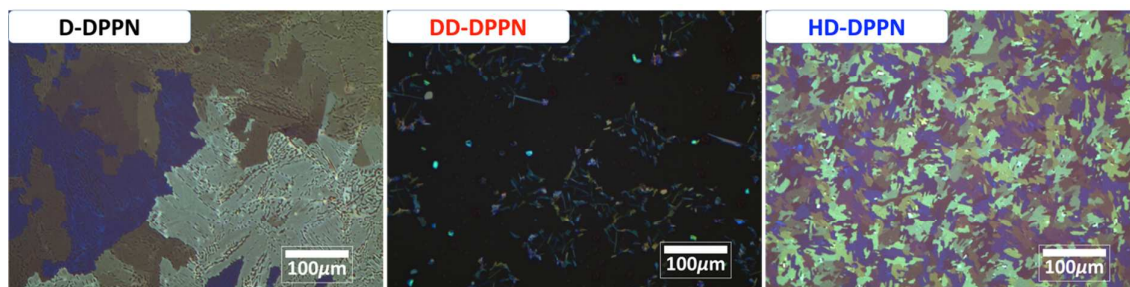


Fig. 10 Polarized microscope images of D-DPPN, DD-DPPN and HD-DPPN thin films after 100-°C annealing.

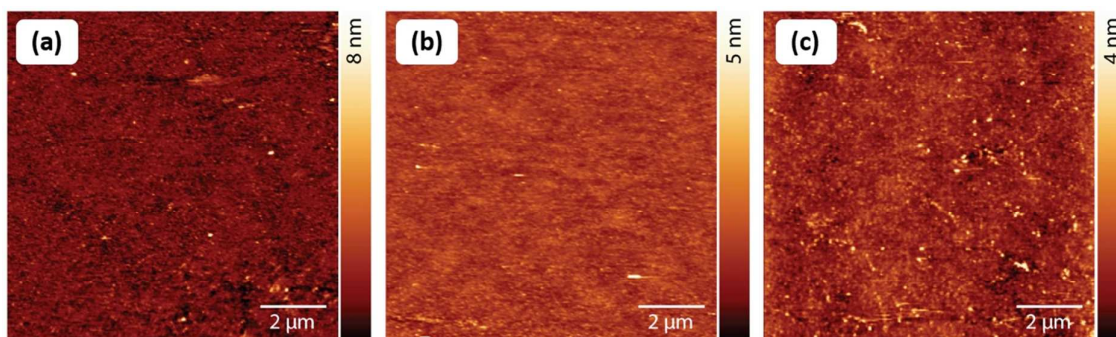


Fig. 11 Contact mode atomic force microscope (AFM) images of D-DPPN (a), DD-DPPN (b) and HD-DPPN (c).

The solid-state microstructural properties of all three DPPN materials D-DPPN, DD-DPPN and HD-DPPN using thin films were studied by using optical microscopy and atomic force microscopy (AFM). The optical micrographs and AFM images of these materials are shown in **Fig. 10** and **Fig. 11** respectively. It is clearly observed from the polarized microscope images in Fig. 10 that all three monomers are crystalline but exhibit different crystal domain sizes after annealing at 100 °C; that is likely the main reason for the differences in hole mobility values. D-DPPN exhibits the largest crystal domain size of up to several hundreds of micrometres that may be caused by the low crystallinity temperature from DSC analysis that allows sufficient time to form large scale of crystal domain and thus the highest hole mobility of $0.019 \text{ cm}^2 \text{ V}^{-1} \text{ s}^{-1}$. DD-DPPN shows *ca.* 100 micrometres of crystal domain size and $0.012 \text{ cm}^2 \text{ V}^{-1} \text{ s}^{-1}$ of hole mobility, while for HD-DPPN, the crystal domain size is only 10-40 micrometres, which causes poor hole mobility in OFET device. After annealing at 150 °C (see Figure S11 in supporting information), recrystallization of the films may cause disconnection between particles and thus the OFET devices did not work under this condition. From the AFM images in Fig. 11, all the thin films show flat, uniform surfaces with similar root-mean-square roughnesses of 0.52 nm for D-DPPN, 0.33 nm for DD-DPPN and 0.42 nm for HD-DPPN after 100-oC annealing.

Conclusions

A new DPP family member, naphthalene flanked diketopyrrolopyrrole (DPPN), was designed and synthesized for the first time. Both straight and branched side chains were attached to the DPP core and the effects of these side chains were studied in detail. We found that the side chains have little influence on the thermal properties and solution absorption. However, different side chains appear to cause different molecular aggregations as indicated in the XRD patterns; the thin film absorption spectra, solid-state emission spectra and HOMO and LUMO energy levels also show large differences. Encouragingly, upon fabricating thin film OFET devices using spin coating, these new DPP monomers exhibit a promising hole mobility of $0.019 \text{ cm}^2 \text{ V}^{-1} \text{ s}^{-1}$ for D-DPPN, $0.0012 \text{ cm}^2 \text{ V}^{-1} \text{ s}^{-1}$ for DD-DPPN and $0.0008 \text{ cm}^2 \text{ V}^{-1} \text{ s}^{-1}$ for HD-DPPN after $100 \text{ }^\circ\text{C}$ annealing. It is important to note that the reported charge carrier mobility value in current work is only for the naphthalene flanked extended conjugated core without any further functionalization. These preliminary results suggest that naphthalene-flanked DPP represents a promising building block for designing new solution-processable organic semiconductors for flexible and printed electronics. The initial insights clearly demonstrate a great potential of this moiety and open a new research avenue in DPP area. Further synthesis of DPPN-containing small molecules and their donor-acceptor polymers is currently under way in our laboratory.

Experimental Section:

Materials and Instruments: All starting materials were purchased commercially as analytical reagents and used directly without any further purification. Distillation prior to use purified all solvents. Reactions were conducted under an atmosphere of argon and monitored

by thin layer chromatography (TLC). ^1H NMR and ^{13}C NMR were obtained with a Bruker 600 spectrometer. The HRMS spectra of final compounds were carried out on a LTQ XL Ion Trap instrument. TGA analysis was performed using a Pegasus Q500TGA thermogravimetric analyser under nitrogen atmosphere at a heating rate of $10\text{ }^\circ\text{C min}^{-1}$. DSC measurements were conducted under nitrogen using a Chimaera instrument Q100 DSC. Photoelectron spectroscopy in air (PESA) measurements was conducted using on an AC-2 photoelectron spectrometer (Riken-Keiki Co.). AFM images were collected using an NT-MDT Solver Pro AFM equipped with Budget Sensors cantilevers with a resonant frequency of 150 kHz, a spring constant of 5 N/m, and a length of 125 μm . DFT calculations were performed in Gaussian 09 using the B3LYP functional and the LANL2DZ basis set. The PCM model of the chloroform solvent was used. Absorption spectra were computed using TD-DFT considering the first six excited states.

Photophysical Measurements: Absorption spectra were recorded at room temperature using a Perkin Elmer Lambda 35 UV/Vis spectrometer. Uncorrected steady state emission and excitation spectra were recorded from air-equilibrated solutions on an Edinburgh FLSP980 spectrometer equipped with a 450 W Xenon arc lamp, double excitation and double emission monochromators and a Peltier cooled Hamamatsu R928P photomultiplier tube (185-850 nm) as well as a Hamamatsu R5509-42 photomultiplier for detection of NIR radiation (spectra range 800-1400 nm). Emission and excitation spectra were corrected for source intensity (lamp and grating) and emission spectral response (detector and grating) by a calibration curve supplied with the instrument. According to the approach described by Demas and Crosby⁶⁴, luminescence quantum yields were measured in optically dilute solutions (O.D. < 0.1 at excitation wavelength) obtained from absorption spectra on a wavelength scale [nm] and compared to the reference emitter by the following equation:

$$\Phi_x = \Phi_r \left[\frac{A_r(\lambda_r)}{A_x(\lambda_x)} \right] \left[\frac{I_r(\lambda_r)}{I_x(\lambda_x)} \right] \left[\frac{n_x^2}{n_r^2} \right] \left[\frac{D_x}{D_r} \right]$$

where A is the absorbance at the excitation wavelength λ , I is the intensity of the excitation light at the excitation wavelength λ , n is the refractive index of the solvent, D is the integrated intensity of the luminescence and Φ is the quantum yield. The subscripts r and x refer to the reference and the sample, respectively. The quantum yield determinations were performed at identical excitation wavelength for the sample and the reference, therefore cancelling the $I_r(\lambda_r)/I_x(\lambda_x)$ term in the equation. The synthesised species were measured against an air-equilibrated aqueous solution of quinine sulfate in 0.1 M H₂SO₄ used as reference ($\Phi_r = 0.546$).⁶⁵ Emission lifetimes (τ) were determined with the time-correlated single photon counting (TCSPC) technique with the same Edinburgh FLSP920 spectrometer using pulsed picosecond LEDs (EPLD 360, FWHM < 800 ps) as the excitation source and the above-mentioned R928P PMT as detector. The goodness of fit was assessed by minimising the reduced χ^2 function and by visual inspection of the weighted residuals. The dichloromethane used for the preparation of the solutions for photophysical investigations was of spectrometric grade, and was degassed using freeze-pump-thaw technique. The prepared solution was filtered through a 0.2 mm syringe filter before measurement. Experimental uncertainties are estimated to be $\pm 8\%$ for lifetime determinations, $\pm 20\%$ for quantum yields, ± 2 nm and ± 5 nm for absorption and emission peaks.

Powder XRD (X-ray Diffraction) Analysis: The samples were dried overnight in an oven at 40 °C. Following drying, the samples were front pressed into low background quartz sample holders. Powder X-Ray diffraction patterns were acquired using a PANalytical X'Pert Pro MPD in parallel beam mode with a cobalt (Co, $K_{\alpha 1} = 1.789010$ Å) source operating at 40 kV and 40 mA. X-ray diffraction patterns were collected from 3-90° 2 θ at a step size of 0.02° for 1 hour. Incident optics included a parabolic mirror, 0.04 radian Soller slit, a 20 mm mask and

a 0.5° fixed divergence slit. The receiving optics included a 0.09° parallel plate collimator and 0.04 radian Soller slits. The samples were spun during data acquisition.

Grazing Incidence X-ray Diffraction (GIXRD): Grazing incidence X-ray diffraction (GIXRD) patterns were acquired using a Rigaku SmartLab diffractometer (Cu source, 40 kV 40 mA) operating in parallel beam mode with a Hypix 3000 detector. The incidence angle (ω) was fixed to 0.5° during data collection. The incident optics consisted of 5° Soller slits, 5 mm incident slit and a fixed divergence slit at 0.075 mm. Receiving optics included a 0.114° collimator and a 20 mm receiving slit. Patterns were collected at 0.75 deg·min⁻¹ at a step size of 0.01° from 2 - 50° 2 θ .

Device Fabrication: OFET devices were fabricated in a Top-Gate/Bottom-Contact structure. Glass substrates were employed, and a lithographed electrode (Au/Ni = 13 nm/3 nm) was used as the source and drain electrodes. The glass substrates were sequentially cleaned with acetone, DI water, and isopropanol, and oven dried at 110 °C for 1 h. After drying, the substrates were treated with UV/Ozone for 30 min and then moved into a N₂ filled glove box. DPPN derivatives, D-DPPN, DD-DPPN and HD-DPPN, (3 mg/ml in Chlorobenzene) was spin-coated at 2000 rpm and annealed at 100 °C (below melting point) or 150 °C (over melting point) for 1 h. CYTOP was spin coated on to the organic semiconductor as the dielectric layer (~500 nm) and annealed at 90 °C for 1h. Al (50 nm) was used for the gate electrode and was thermally evaporated under vacuum (~10⁻⁶ Torr). Electrical characterization was measured under nitrogen using a Keithley semiconductor parametric analyzer (Keithley 4200-SCS) under nitrogen atmosphere in glove box. Hole mobility (μ) was determined using $I_{ds} = (WC_i/2L) \times \mu \times (V_g - V_{th})^2$ in the saturation regime.

Synthesis:

Synthesis of 3,6-di(naphthalen-2-yl)-2,5-dihydropyrrolo[3,4-c]pyrrole-1,4-dione (NH-DPPN):

A three-neck round-bottom flask connected to a condenser was charged with a stir bar and

potassium tert-butoxide (3.9 g, 35.1 mmol) with argon protection. Naphthalene-2-carbonitrile (6 g, 39 mmol) and t-amyl alcohol (34 mL) were added in one portion. The mixture was progressively warmed to 120 °C for about half an hour. A solution of diisopropyl succinate (3.2 g, 16 mmol) in t-amyl alcohol (10 mL) was subsequently added dropwise over 1 h and then the mixture was kept stirring for another 2 h at the same temperature. The reaction mixture was then cooled to 65 °C and precipitated into acidic MeOH (220 mL MeOH and 11 mL conc. HCl) gradually. After stirring for half an hour, the resulting suspension was filtered, washed with hot methanol and water twice each and dried in vacuum to yield the red solid NH-DPPN (3.8 g, 61%), which was used directly in the subsequent reactions without further purification.

Synthesis of 2,5-didecyl-3,6-di(naphthalen-2-yl)-2,5-dihydropyrrolo[3,4-c]pyrrole-1,4-dione

(D-DPPN): NH-DPPN (0.84 g, 2.16 mmol), potassium tert-butoxide (485 mg, 4.32 mmol) were suspended in anhydrous N,N-dimethylformamide (25 mL) with argon protection. The mixture was stirred for 1h at room temperature and then heated to 60 °C, a solution of *n*-decyl bromide (2.9 g, 12.96 mmol) in N,N-dimethylformamide (5 mL) was added dropwise over 1 h. After stirring for 20 h, the reaction mixture was filtered and the organic layer was diluted with 50 mL of ethyl acetate and washed with water and brine several times. The organic phase was then dried over sodium sulfate and concentrated to obtain crude product which was purified by column chromatography on silica gel using hexane: ethyl acetate = 10:1 as eluent and then recrystallization in methanol to obtain orange solid D-DPPN (480 mg, 33%).

¹H NMR (600 MHz, CDCl₃) δ (ppm) 8.36 (s, 2H), 7.93 (d, *J* = 7.8 Hz, 2H), 7.85-7.79 (m, 6H), 7.57-7.51 (m, 4H), 3.87 (t, *J* = 7.8 Hz, *J* = 7.2 Hz, 4H), 1.62 (m, 4H), 1.29-1.16 (m, 28H), 0.88 (t, *J* = 7.2 Hz, *J* = 7.2 Hz, 6H).

^{13}C NMR (151 MHz, CDCl_3) δ (ppm) 162.79, 148.53, 134.23, 132.82, 129.43, 128.96, 128.42, 127.76, 126.69, 125.61, 125.07, 110.13, 41.97, 31.87, 29.46, 29.45, 29.41, 29.25, 29.05, 26.74, 22.67, 14.14.

HRMS $[\text{M}+\text{H}]^+$ m/z calcd. 669.4342 found 669.4413.

Synthesis of 2,5-didodecyl-3,6-di(naphthalen-2-yl)-2,5-dihydropyrrolo[3,4-c]pyrrole-1,4-dione (DD-DPPN): NH-DPPN: (1 g, 2.57 mmol), potassium tert-butoxide (577 mg, 5.14 mmol) were suspended in anhydrous N,N-dimethylformamide (28 mL) with argon protection. The mixture was stirred for 1 h at room temperature and then heated to 60 °C, a solution of *n*-dodecyl bromide (3.8 g, 15.42 mmol) in N,N-dimethylformamide (6 mL) was added dropwise over 1 h. After stirring for 20 h, the reaction mixture was filtered and the organic layer was diluted with 50 mL of ethyl acetate and washed with water and brine several times. The organic phase was then dried over sodium sulfate and concentrated to obtain crude product which was purified by column chromatography on silica gel using hexane: ethyl acetate = 10:1 as eluent and then recrystallization in methanol to obtain red solid DD-DPPN (460 mg, 25%).

^1H NMR (600 MHz, CDCl_3) δ (ppm) 8.38 (s, 2H), 7.96 (d, $J = 7.8$ Hz, 2H), 7.91-7.85 (m, 6H), 7.60-7.55 (m, 4H), 3.88 (t, $J = 7.8$ Hz, $J = 7.2$ Hz, 4H), 1.65 (m, 4H), 1.31-1.17 (m, 36H), 0.89 (t, $J = 7.2$ Hz, $J = 7.2$ Hz, 6H).

^{13}C NMR (151 MHz, CDCl_3) δ (ppm) 162.83, 148.51, 134.30, 132.89, 129.42, 128.98, 128.53, 127.83, 127.80, 126.78, 125.65, 125.08, 110.20, 42.06, 31.92, 29.61, 29.60, 29.52, 29.46, 29.34, 29.06, 26.75, 22.70, 14.14.

HRMS $[\text{M}+\text{H}]^+$ m/z calcd. 725.4968 found 725.5039.

Synthesis of 2,5-bis(2-hexyldecyl)-3,6-di(naphthalen-2-yl)-2,5-dihydropyrrolo[3,4-c]pyrrole-1,4-dione (HD-DPPN): NH-DPPN (0.96 g, 2.47 mmol), potassium tert-butoxide (554 mg, 4.94 mmol) were suspended in anhydrous N,N-dimethylformamide (25 mL) with argon

protection. The mixture was stirred for 1 h at room temperature and then heated to 60 °C, a solution of 2-hexyldecyl bromide (4.5 g, 14.82 mmol) in N,N-dimethylformamide (5 mL) was added dropwise over 1 h. After stirring for 20 h, the reaction mixture was filtered and the organic layer was diluted with 50 mL of ethyl acetate and washed with water and brine several times. The organic phase was then dried over sodium sulfate and concentrated to obtain crude product which was purified by column chromatography on silica gel using hexane: ethyl acetate = 10:1 as eluent and then recrystallization in methanol to obtain orange solid HD-DPPN (370 mg, 18%).

^1H NMR (600 MHz, CDCl_3) δ (ppm) 8.32 (s, 2H), 7.92 (d, $J = 7.8$ Hz, 2H), 7.80 (m, 6H), 7.57-7.51 (m, 4H), 3.87 (d, $J = 7.2$ Hz, 4H), 1.52 (m, 2H), 1.28-0.98 (m, 48H), 0.87 (t, $J = 7.2$ Hz, $J = 7.2$ Hz, 6H), 0.80 (t, $J = 7.2$ Hz, $J = 7.2$ Hz, 6H).

^{13}C NMR (151 MHz, CDCl_3) δ (ppm) 162.88, 148.70, 134.17, 132.80, 129.25, 128.87, 128.37, 127.77, 127.65, 126.65, 125.96, 125.08, 110.06, 45.33, 36.98, 31.88, 31.70, 31.28, 31.27, 29.86, 29.52, 29.47, 29.27, 26.06, 26.01, 22.67, 22.59, 14.14, 14.08.

HRMS $[\text{M}+\text{H}]^+$ m/z calcd. 837.6220 found 837.6292.

Conflicts of interest

There are no conflicts to declare.

Acknowledgement

Qian Liu is thankful to QUT for offering here QUTPRA scholarship to conduct his research.

P.S. is thankful to QUT for the financial support from the Australian Research Council (ARC) for the Future Fellowship (FT130101337) and QUT core funding (QUT/322120-0301/07).

S.M. is supported by the Ministry of Education of Singapore. Some of the data reported in

this paper were obtained at the Central Analytical Research Facility (CARF) operated by the Institute for Future Environments (QUT). Access to CARF is supported by generous funding from the Science and Engineering Faculty (QUT).

References

- 1 A. Brown, A. Pomp, C. Hart and D. De Leeuw, *Science*, 1995, **270**, 972.
- 2 F. Cicoira and C. Santato, *Adv. Funct. Mater.*, 2007, **17**, 3421-3434.
- 3 B. Crone, A. Dodabalapur, A. Gelperin, L. Torsi, H. Katz, A. Lovinger and Z. Bao, *Appl. Phys. Lett.*, 2001, **78**, 2229-2231.
- 4 B. Crone, A. Dodabalapur, Y. Lin and R. Filas, *Nature*, 2000, **403**, 521.
- 5 G. H. Gelinck, H. E. A. Huitema, E. van Veenendaal, E. Cantatore, L. Schrijnemakers, J. B. P. H. van der Putten, T. C. T. Geuns, M. Beenhakkers, J. B. Giesbers and B.-H. Huisman, *Nat. Mater.*, 2004, **3**, 106.
- 6 B. Wang, T. P. Huynh, W. Wu, N. Hayek, T. T. Do, J. C. Cancilla, J. S. Torrecilla, M. M. Nahid, J. M. Colwell, O. M. Gazit, S. R. Puniredd, C. R. McNeill, P. Sonar and H. Haick, *Adv. Mater.*, 2016, **28**, 4012-4018.
- 7 C. B. Nielsen, M. Turbiez and I. McCulloch, *Adv. Mater.*, 2013, **25**, 1859-1880.
- 8 Y. Zhao, Y. Guo and Y. Liu, *Adv. Mater.*, 2013, **25**, 5372-5391.
- 9 Y. Li, S. P. Singh and P. Sonar, *Adv. Mater.*, 2010, **22**, 4862-4866.
- 10 Y. Li, P. Sonar, L. Murphy and W. Hong, *Energy Environ. Sci.*, 2013, **6**, 1684-1710.
- 11 M. Mas-Torrent and C. Rovira, *Chem. Soc. Rev.*, 2008, **37**, 827-838.
- 12 W. Wu, Y. Liu and D. Zhu, *Chem. Soc. Rev.*, 2010, **39**, 1489-1502.
- 13 B. Lim, H. Sun and Y.-Y. Noh, *Dyes Pigm.*, 2017, **142**, 17-23.
- 14 B. Lim, H. Sun, J. Lee and Y.-Y. Noh, *Sci. Rep.*, 2017, **7**, 164.

- 15 Z. Ni, H. Dong, H. Wang, S. Ding, Y. Zou, Q. Zhao, Y. Zhen, F. Liu, L. Jiang and W. Hu, *Adv. Mater.*, 2018, **30**, 1704843.
- 16 I. Kang, H. J. Yun, D. S. Chung, S. K. Kwon and Y. H. Kim, *J. Am. Chem. Soc.*, 2013, **135**, 14896-14899.
- 17 J. Y. Back, H. Yu, I. Song, I. Kang, H. Ahn, T. J. Shin, S.-K. Kwon, J. H. Oh and Y.-H. Kim, *Chem. Mater.*, 2015, **27**, 1732-1739.
- 18 R. S. Ashraf, I. Meager, M. Nikolka, M. Kirkus, M. Planells, B. C. Schroeder, S. Holliday, M. Hurhangee, C. B. Nielsen, H. Sirringhaus and I. McCulloch, *J. Am. Chem. Soc.*, 2015, **137**, 1314-1321.
- 19 P. Sonar, J. Chang, Z. Shi, E. Gann, J. Li, J. Wu and C. R. McNeill, *J. Mater. Chem. C*, 2015, **3**, 9299-9305.
- 20 P. Sonar, J. Chang, Z. Shi, J. Wu and J. Li, *J. Mater. Chem. C*, 2015, **3**, 2080-2085.
- 21 H. Sirringhaus, *Adv. Mater.*, 2005, **17**, 2411-2425.
- 22 H. Chen, Y. Guo, G. Yu, Y. Zhao, J. Zhang, D. Gao, H. Liu and Y. Liu, *Adv. Mater.*, 2012, **24**, 4618-4622.
- 23 P. Cai, Z. Chen, L. Zhang, J. Chen and Y. Cao, *J. Mater. Chem. C*, 2017, **5**, 2786-2793.
- 24 S. Park, B. T. Lim, B. Kim, H. J. Son and D. S. Chung, *Sci. Rep.*, 2014, **4**, 5482.
- 25 H. Okamoto, N. Kawasaki, Y. Kaji, Y. Kubozono, A. Fujiwara and M. Yamaji, *J. Am. Chem. Soc.*, 2008, **130**, 10470-10471.
- 26 T. Yamamoto and K. Takimiya, *J. Am. Chem. Soc.*, 2007, **129**, 2224-2225.
- 27 J.-I. Park, J. W. Chung, J.-Y. Kim, J. Lee, J. Y. Jung, B. Koo, B.-L. Lee, S. W. Lee, Y. W. Jin and S. Y. Lee, *J. Am. Chem. Soc.*, 2015, **137**, 12175-12178.
- 28 K. Niimi, S. Shinamura, I. Osaka, E. Miyazaki and K. Takimiya, *J. Am. Chem. Soc.*, 2011, **133**, 8732-8739.

- 29 J. Shin, T. R. Hong, T. W. Lee, A. Kim, Y. H. Kim, M. J. Cho and D. H. Choi, *Adv. Mater.*, 2014, **26**, 6031-6035.
- 30 T. Lei, Y. Cao, X. Zhou, Y. Peng, J. Bian and J. Pei, *Chem. Mater.*, 2012, **24**, 1762-1770.
- 31 K. Shi, J. Y. Wang and J. Pei, *Chem. Rec.*, 2015, **15**, 52-72.
- 32 S. Fall, L. Biniek, Y. Odarchenko, D. V. Anokhin, G. de Tournadre, P. Lévêque, N. Leclerc, D. A. Ivanov, O. Simonetti and L. Giraudet, *J. Mater. Chem. C*, 2016, **4**, 286-294.
- 33 C. Kanimozhi, N. Yaacobi-Gross, E. K. Burnett, A. L. Briseno, T. D. Anthopoulos, U. Salzner and S. Patil, *Phys. Chem. Chem. Phys.*, 2014, **16**, 17253-17265.
- 34 G. Adam, A. Pivrikas, A. M. Ramil, S. Tadesse, T. Yohannes, N. S. Sariciftci and D. A. Egbe, *J. Mater. Chem.*, 2011, **21**, 2594-2600.
- 35 R. R. Jadhav, N. Camaioni, K. Oppelt, F. Tinti, M. Gazzano, V. Fattori, P. P. Wadgaonkar, S. Rathgeber, H. Hoppe and D. A. Egbe, *RSC Adv.*, 2016, **6**, 51642-51648.
- 36 B. Fu, J. Baltazar, A. R. Sankar, P. H. Chu, S. Zhang, D. M. Collard and E. Reichmanis, *Adv. Funct. Mater.*, 2014, **24**, 3734-3744.
- 37 A. Han, G. K. Dutta, J. Lee, H. R. Lee, S. M. Lee, H. Ahn, T. J. Shin, J. H. Oh and C. Yang, *Adv. Funct. Mater.*, 2015, **25**, 247-254.
- 38 J. H. Dou, Y. Q. Zheng, T. Lei, S. D. Zhang, Z. Wang, W. B. Zhang, J. Y. Wang and J. Pei, *Adv. Funct. Mater.*, 2014, **24**, 6270-6278.
- 39 S. G. Surya, S. S. Nagarkar, S. K. Ghosh, P. Sonar and V. R. Rao, *Sens. Actuators B: Chem.*, 2016, **223**, 114-122.
- 40 Y. Zhou, S.-T. Han, P. Sonar and V. Roy, *Sci. Rep.*, 2013, **3**, 2319.

- 41 Y. Zhou, S.-T. Han, Y. Yan, L. Zhou, L.-B. Huang, J. Zhuang, P. Sonar and V. Roy, *Sci. Rep.*, 2015, **5**, 10683.
- 42 A. T. Yiu, P. M. Beaujuge, O. P. Lee, C. H. Woo, M. F. Toney and J. M. Frechet, *J. Am. Chem. Soc.*, 2012, **134**, 2180-2185.
- 43 Y. Li, P. Sonar, S. P. Singh, W. Zeng and M. S. Soh, *J. Mater. Chem.*, 2011, **21**, 10829-10835.
- 44 I. Meager, R. S. Ashraf, S. Mollinger, B. C. Schroeder, H. Bronstein, D. Beatrup, M. S. Vezie, T. Kirchartz, A. Salleo, J. Nelson and I. McCulloch, *J. Am. Chem. Soc.*, 2013, **135**, 11537-11540.
- 45 W. Li, K. H. Hendriks, A. Furlan, M. M. Wienk and R. A. Janssen, *J. Am. Chem. Soc.*, 2015, **137**, 2231-2234.
- 46 L. Huo, J. Hou, H.-Y. Chen, S. Zhang, Y. Jiang, T. L. Chen and Y. Yang, *Macromolecules*, 2009, **42**, 6564-6571.
- 47 K. Gao, L. Li, T. Lai, L. Xiao, Y. Huang, F. Huang, J. Peng, Y. Cao, F. Liu and T. P. Russell, *J. Am. Chem. Soc.*, 2015, **137**, 7282-7285.
- 48 T. Ma, K. Jiang, S. Chen, H. Hu, H. Lin, Z. Li, J. Zhao, Y. Liu, Y.-M. Chang, C.-C. Hsiao and H. Yan, *Adv. Energy Mater.*, 2015, **5**, 1501282.
- 49 Y. Li, P. Sonar, S. P. Singh, M. S. Soh, M. van Meurs and J. Tan, *J. Am. Chem. Soc.*, 2011, **133**, 2198-2204.
- 50 J. Jung, W. Lee, C. Lee, H. Ahn and B. J. Kim, *Adv. Energy Mater.*, 2016, **6**, 1600504.
- 51 H. Li, T. Earmme, S. Subramaniyan and S. A. Jenekhe, *Adv. Energy Mater.*, 2015, **5**, 1402041.
- 52 K. Kawashima, I. Osaka and K. Takimiya, *Chem. Mater.*, 2015, **27**, 6558-6570.
- 53 C.-E. Tsai, R.-H. Yu, F.-J. Lin, Y.-Y. Lai, J.-Y. Hsu, S.-W. Cheng, C.-S. Hsu and Y.-J. Cheng, *Chem. Mater.*, 2016, **28**, 5121-5130.

- 54 D. Ding, J. Wang, Z. Du, F. Li, W. Chen, F. Liu, H. Li, M. Sun and R. Yang, *J. Mater. Chem. A*, 2017, **5**, 10430-10436.
- 55 D. Liu, C. Gu, J. Wang, D. Zhu, Y. Li, X. Bao and R. Yang, *J. Mater. Chem. A*, 2017, **5**, 9141-9147.
- 56 S. Loser, C. J. Bruns, H. Miyauchi, R. P. Ortiz, A. Facchetti, S. I. Stupp and T. J. Marks, *J. Am. Chem. Soc.*, 2011, **133**, 8142-8145.
- 57 H. Katayama, T. Tawa, S. Ito and M. Yamamoto, *J. Chem. Soc., Faraday Trans.*, 1992, **88**, 2743-2746.
- 58 X. Qiao, X. Wang and Z. Mo, *Synth. Met.*, 2001, **118**, 89-95.
- 59 P. Data, A. Kurowska, S. Pluczyk, P. Zassowski, P. Pander, R. Jedrysiak, M. Czwartosz, L. Otulakowski, J. Suwinski and M. Lapkowski, *J. Phys. Chem. C*, 2016, **120**, 2070-2078.
- 60 M. Jung, Y. Yoon, J. H. Park, W. Cha, A. Kim, J. Kang, S. Gautam, D. Seo, J. H. Cho and H. Kim, *ACS Nano*, 2014, **8**, 5988-6003.
- 61 C.-H. Lee, Y.-Y. Lai, J.-Y. Hsu, P.-K. Huang and Y.-J. Cheng, *Chem. Sci.*, 2017, **8**, 2942-2951.
- 62 A. Kovalenko, C. Yumusak, P. Heinrichova, S. Stritesky, L. Fekete, M. Vala, M. Weiter, N. S. Sariciftci and J. Krajcovic, *J. Mater. Chem. C*, 2017, **5**, 4716-4723.
- 63 J. Dhar, D. P. Karothu and S. Patil, *Chem. Commun.*, 2015, **51**, 97-100.
- 64 J. N. Demasa and G. A. Crosby, *J. Phys. Chem.*, 1968, **48**, 991-1024.
- 65 D. F. Eaton, *Pure & Appl. Chem.*, 1988, **60**, 1107-1114.